Impact of Coating Defects on Performance of Coated Zirconium Cladding

Nuclear Technology Research and Development

Approved for unlimited distribution

Prepared for
U.S. Department of Energy
Tim Graening
Ben Garrison
Kenneth Kane
Kory Linton
Andrew Nelson
Oak Ridge National Laboratory

09/24/2021
M3FT-21OR020202015
ORNL/SPR-2021/2252

SUMMARY

The Advanced Fuels Campaign has made progress in developing an ability to fabricate high quality ‘generic’ chromium coatings applied to commercial nuclear cladding alloys free of the proprietary considerations inherent to the industry materials. The availability of such source material is critical for execution of fundamental studies as well as open collaboration between the national laboratories, within Office of Nuclear Energy programs, and the Nuclear Regulatory Commission. This milestone report provides insights on the impact of processing parameters on the microstructure of 7 micron Cr-coated Zircaloy-4. Coatings were applied using High Power Impulse Magnetron Sputtering (HiPIMS). Scanning electron microscopy was utilized to investigate the overcoating of cladding and cross-sections of the interface. Characterization confirmed that a high quality, continuous coating was achieved. Burst testing was then performed to evaluate the performance of high-quality coatings to coatings that contain known flaws and uncoated materials. Results demonstrated that coatings containing flaws allowing for direct exposure of the base cladding to atmosphere exhibit burst behavior matching that of the uncoated material. However, continuous coatings resulted in measurable improvement. This work will be expanded in FY22 to include a broader set of mechanical property studies and test irradiations.

CONTENTS

FIGURES

TABLES

ACRONYMS

ASTM	American Society for Testing and Materials
ATF	accident-tolerant fuel
BCC	base centered cubic
BISON	a finite element–based nuclear fuel performance code
BWR	boiling water reactor
CTE	coefficient of thermal expansion
CVD	chemical vapor deposition
EBSD	electron backscatter diffraction
EDS	energy-dispersive x-ray spectroscopy
EFTEM	energy-filtered transmission electron microscopy
FEM	finite element method
HAADF	High Angle Annular Dark Field
HFIR	High Flux Isotope Reactor
HiPIMS	high-power impulse magnetron sputtering
IFEL	Irradiated Fuels Examination Facility
LFA	laser flash analysis
LOCA	loss-of-coolant accident
LWR	light-water reactor
MBT	modified burst test
ORNL	Oak Ridge National Laboratory
PVD	physical vapor deposition
PWR	pressurized water reactor
SATS	Severe Accident Test Station
SEM	scanning electron microscopy
STEM	scanning transmission electron microscopy
TEM	transmission electron microscopy
UTS	ultimate tensile strength
XRD	x-ray diffraction
YS	yield strength
ZIRLO	advanced zirconium-based alloy by Westinghouse
Zry-4	Zircaloy-4

IMPACT OF COATING DEFECTS ON PERFORMANCE OF COATED ZIRCONIUM CLADDING

1. INTRODUCTION

Research on accident tolerant fuels (ATF) has started after the Fukushima accident [1–3]. While efforts have been expended on both fuel and cladding ATF concepts, the bulk of work has been devoted to improved cladding. The overarching goal of these approaches is to extend the coping time available during a severe accident before any event would result in release of radioactivity to the public. The most basic ATF cladding concept is obtained by applying a thin coating of highly corrosion-resistant material on the surface of a licensed zirconium cladding alloy. This thin coating is intended to not interfere with the neutronic or mechanical performance of the base cladding under normal operating conditions. Different coating materials, thicknesses, coating processes, process parameters, and testing methods have an impact on the microstructure and mechanical properties and therefore on the results of the applied investigation methods. These challenges have motivated an initial focus on demonstrating that the presence of coatings do not perturb the critical performance benchmarks of uncoated material. Ongoing lead test assembly irradiations of coated zirconium concepts in commercial reactions is intended to establish baseline performance in this regard in the coming years.

The next evolution of fuel vendor and plant operator interest will come in efforts to take credit for the performance benefits imparted by the coating. This is a greater challenge, as a deeper understanding of how coating properties and performance impact those of the cladding in its entirety is needed [4]. The list of potential research focuses within the field of coating performance under irradiation is extensive; an understanding of the most critical properties needs to be prioritized to develop repeatable and less time consuming methods. A large variety of methods have been developed to investigate coatings for cladding materials and their mechanical properties [5–9] and coated zirconium cladding concepts have grown to become prioritized approaches of industry ATF efforts.

The challenge for the research and regulatory community is that vendor coating concepts are all proprietary, and highly bound by restrictions on data distribution. Many Advanced Fuels Campaign (AFC) national laboratories are actively collecting data for all U.S. fuel vendors coated cladding concepts, but dissemination and discussion of these results in an open format is not possible. This limitation has prompted AFC to invest in independently sourced coatings free of these restrictions. The focus of this work is production of materials at scales necessary for execution of fundamental research to understand the impacts of coatings on critical performance issues, not development of processes applicable to commercial fuel cladding fabrication. Success in producing these coated Zr cladding materials will enable material investigations, basic property studies, failure modes, and other attributes for discussion in the open literature. The availability of this data will enhance technical discussion across vendor teams and dialogue with regulatory bodies.

This report focuses on the microstructure characterization of FY21 Cr-coating with a thickness of a 6 μm as created by High Power Impulse Magnetron Sputtering (HiPIMS) on Zry-4 tubes.

Chromium coatings have been chosen for this study due to their outstanding corrosion resistance under normal operating temperatures and a good oxidation resistance under accident conditions. While not all U.S. vendors use Cr metal coatings, it is more common than other Cr-containing coating materials and represents the best choice of an initial 'generic' coating material for initial optimization studies.

HiPIMS parameters like the utilized atmosphere, target average power, pulse duty cycle and pulse width, as well as peak voltage and current are just a few parameters which have a direct impact on the created coating and its adhesion on the substrate material. To show how those parameters impact the coating microstructure Figure 1 shows the dependency of the substrate temperature, kinetic energy of ions, and the deposition rate [10]. It also demonstrates the ability of HiPIMS to tailor the coating microstructure so that the coating excels in crucial areas such as the residual stress state of the coating and thermal and irradiation creep. The deposition temperature and the substrate bias voltage have proven to be important parameters to control and achieve optimized coating properties. The impact of the substrate bias on the interface mixing, the surface roughness, adhesion, and island formation has been simulated in a recent publication [11].

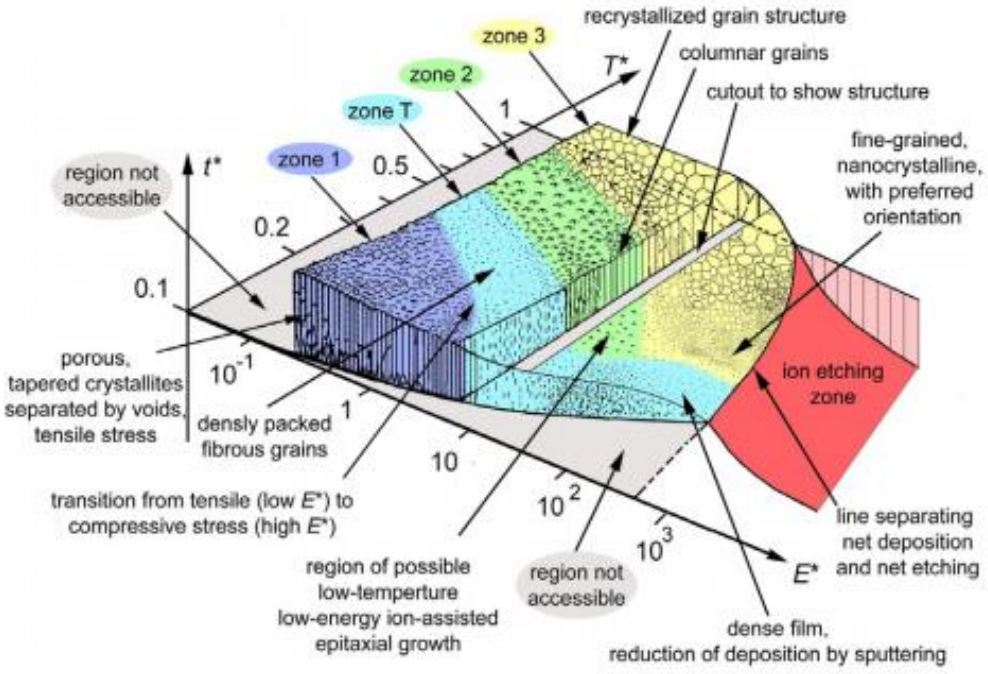

Figure 1. Generalized Structure Zone Diagram in dependence of temperature T and energy E [10].

This report provides preliminary insights into the microstructure of (high-power impulse magnetron sputtering) HiPIMS coated Cr on Zircaloy in relation to different substrate bias voltages, while all other coating properties were kept constant. This work enabled burst tests of coated cladding with both continuous and compromised coatings as well as uncoated material to evaluate the coating impact in potential accident scenarios [9,12–14].

2. MATERIALS

2.1 ZIRCALOY-4 CLADDING MATERIAL

Zry-4 is widely used as a standard for nuclear research due to its large database of well-characterized material properties for comparison, its relative lack of proprietary restrictions, and its relative similarity to the newer Zr-based alloys. ORNL procured several hundred meters of Zry-4 from Cameco Fuel Manufacturing (Port Hope, Ontario, Canada) in FY20. The material was stress relieved annealed and conformed to the typical geometry of a PWR cladding, conforming to ASTM B353-12 and stress relieved per ASTM B350-11, with a surface finish of 0.81 micrometer R-average (Ra) or better [21]. Product certifications are on file at ORNL.

The tubes were cut into ~300 mm segments for handling purposes. The geometry and chemical composition of Zircaloy-4 tubes are shown in Table 1. As shown in recent reports [15,16] the surface finish of Zry-4 tubes was not smooth enough for direct coating on the surface of as-received material. Adhesion of the coating was not sufficient, and the directional growth of the coating during the HiPIMS process led to cracks and uncoated areas. To prevent that, Zry-4 tubes were subsequently polished to a 3-micron finish before coating. Optical microscopy images of polished but not coated surfaces are shown in Figure 2 from as-received condition to a 3 micron finish.

Table 1. Dimension and nominal chemical composition of Zircaloy-4.

Parameter	Zircaloy-4[a]
Length, mm	30.48
Width, mm	9.50
Thickness, mm	0.56
Zr, wt.%	Balance
Sn, wt.%	1.20–1.45
Fe + Cr + Ni, wt.%	0.37 (no Ni)
Cr, wt.%	0.07–0.13
Ni, wt.%	-

[a]ASTM B353

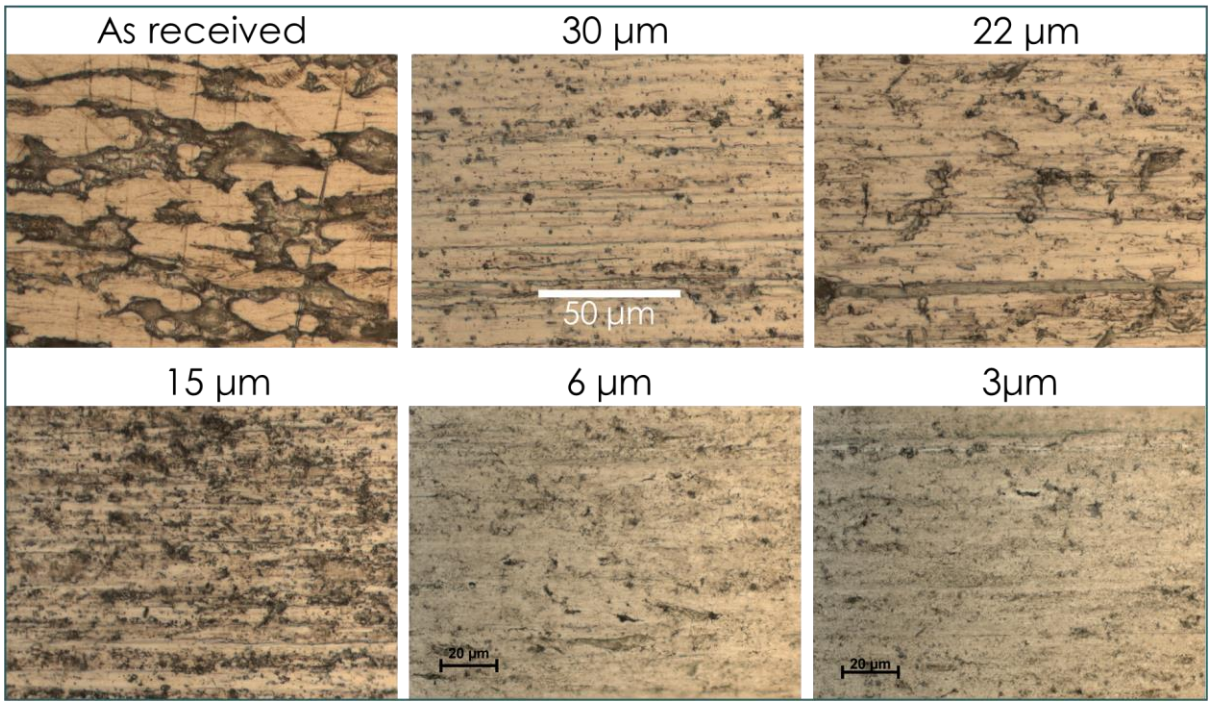

Figure 2 Optical images of the tube surface in as-received and subsequently polished condition.

2.2 COATING FABRICATION

The polished tubes were cleaned with ethanol and methanol in an ultrasonic bath and send to Acree Technologies Inc. in California to apply a 6 micron Cr-coating using a HiPIMS process. Before the mounting of the 12" Zry-tubes in the PVD coating machine, the tubes were again cleaned using an ultrasonic cleaner and isopropanol. After mounting, a plasma cleaning step at around -1000 V for 60 minutes was conducted to clean the surface of the cladding tubes prior to the coating process. The selected temperature was about 190 to 210 °C. To increase the adhesion in comparison with the coating presented in a recent report [15], a substrate bias of around -1000 V was applied during the initial 10 minutes of the coating process. After that initial step, the substrate voltage bias was set to -100, -150, and -200 V for seven tubes each. Applying a substrate bias during the coating process allows to control the bombardment energy of the ions of the film forming material, which enables control over properties like grain size and texture of the coating. A growth rate of around 1 µm per hour was achieved. The relatively low coating temperature was chosen to ensure that thermal expansion differences between the Cr coating and the Zircaloy cladding material is not negatively impacting the properties of the coating, while ensuring to create a microstructure similar to zone T or zone 2 shown in Figure 1. HiPIMS PVD coating growth occurs very directional and mirrors the substrate surface [17]. Figure 3 shows the impact of a bad adhesion of a coating applied with a low substrate voltage bias of -35V on a tube with a high local peak roughness value [15]. Although this effort was ultimately unsuccessful in obtaining a continuous coating, it did supply material where a high fraction of the surface was coated with discrete defective points. This material was used for burst testing of discontinuous coatings described in Section 4.

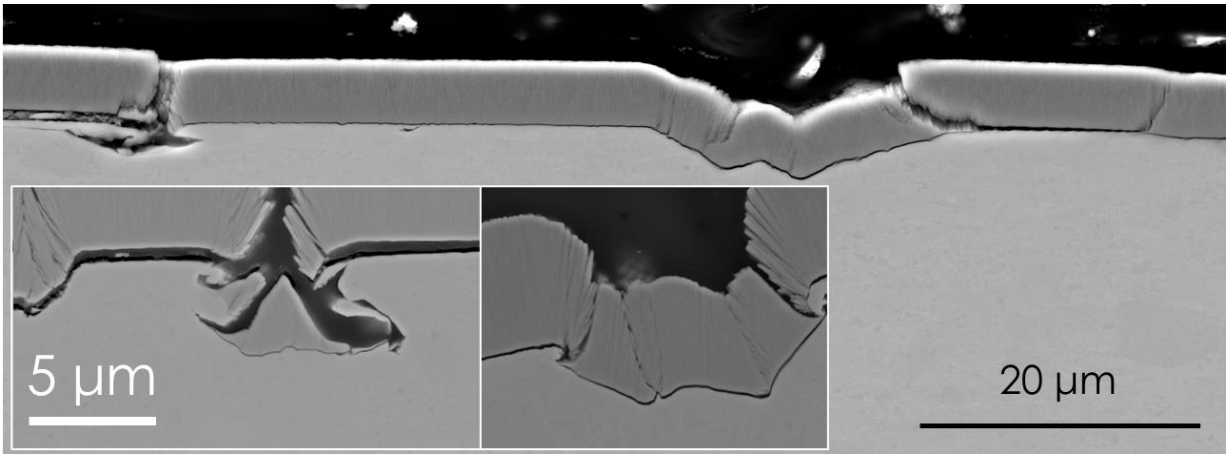

Figure 3 Rough substrate surface and a low substrate bias voltage led to a low adhesion in previous studies [15].

3. MICROSTRUCTURE INVESTIGATION

To avoid a low adhesion and cracking of the applied coating, polishing the surface as shown in Figure 2 in the previous section and increasing the substrate bias was necessary. In addition, to create a strong bond between coating and cladding a very high substrate bias during the first ten minutes of the coating process of -1000V was chosen to overcome the challenge of bad adhesion and cracked coatings. An assemblage of uncoated, polished, and coated tubes is shown in comparison in Figure 4. From the macroscopic image, it becomes clear that the Cr bonding was successful. The color between the as-received and polished condition changed to a typical Cr-color after the HiPIMS process.

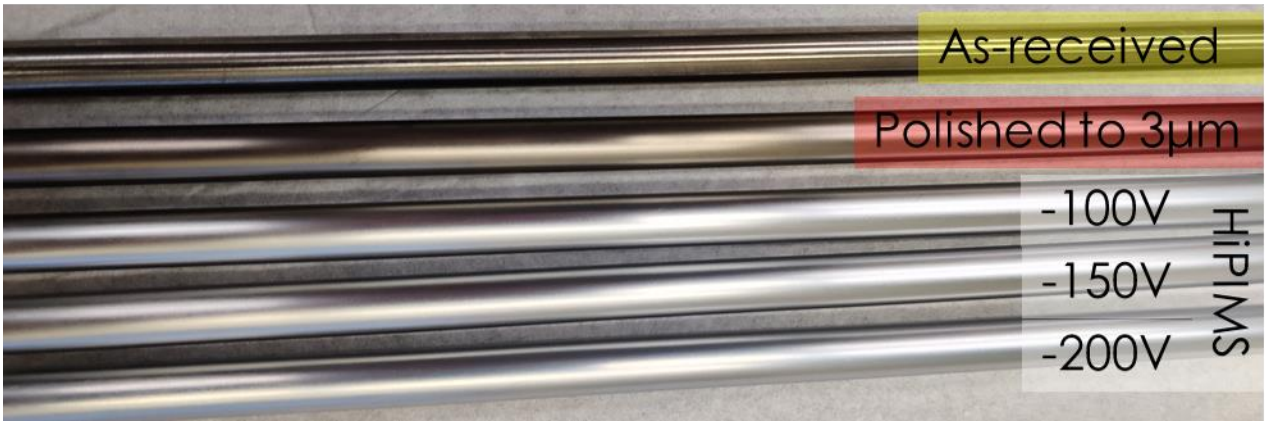

Figure 4 As-received, polished, and Cr-coated tubes in comparison with each other.

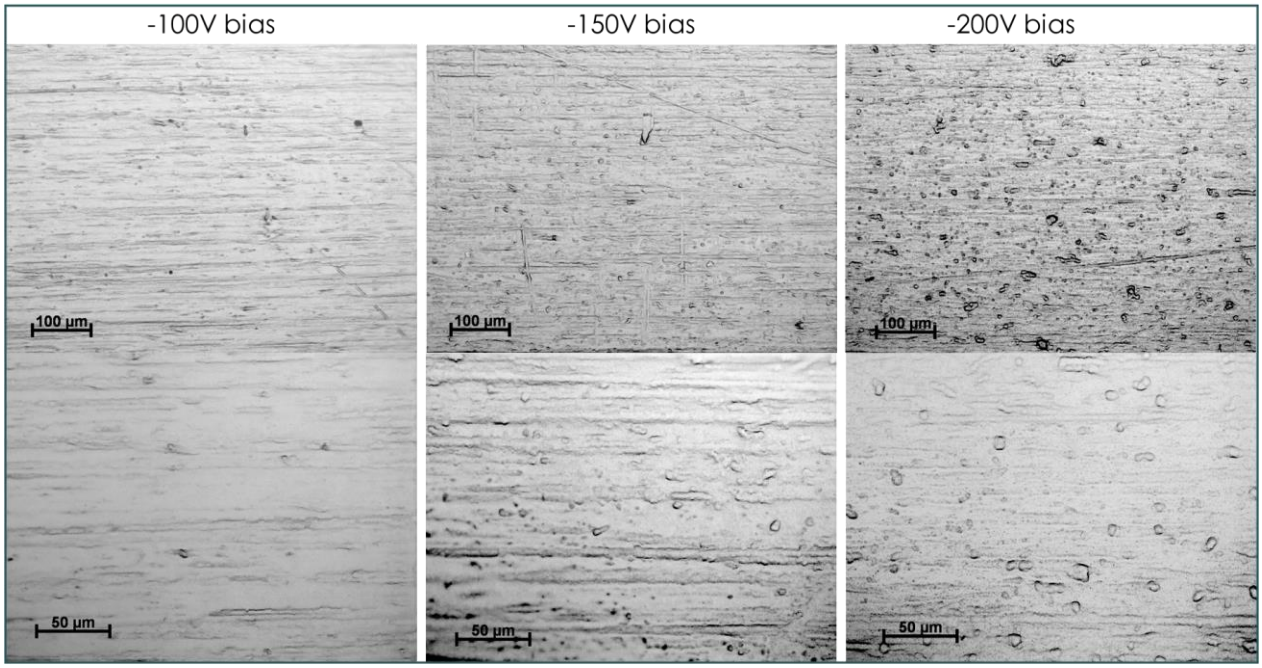

Figure 5 Optical Microscopy of Cr-coated material reveals no cracks. The coating is mirroring the surface of the cladding shown in Figure 2.

Large areas of the coated material were investigated using optical microscopy to search for potential cracks or adhesion defects. None of those defects were found using microscopy, however some coated tubes with -150 V bias voltage exhibited a lower adhesion of the coating in comparison with the -100V and -200V samples. On some of those tubes the coating was peeling off when the material was received from the vendor. To investigate the phenomena, radial and axial SEM images were recorded. The results of those investigations for the -100, -150, and -200 V substrate bias voltages are presented in Figure 6, Figure **7**, and Figure 9, respectively.

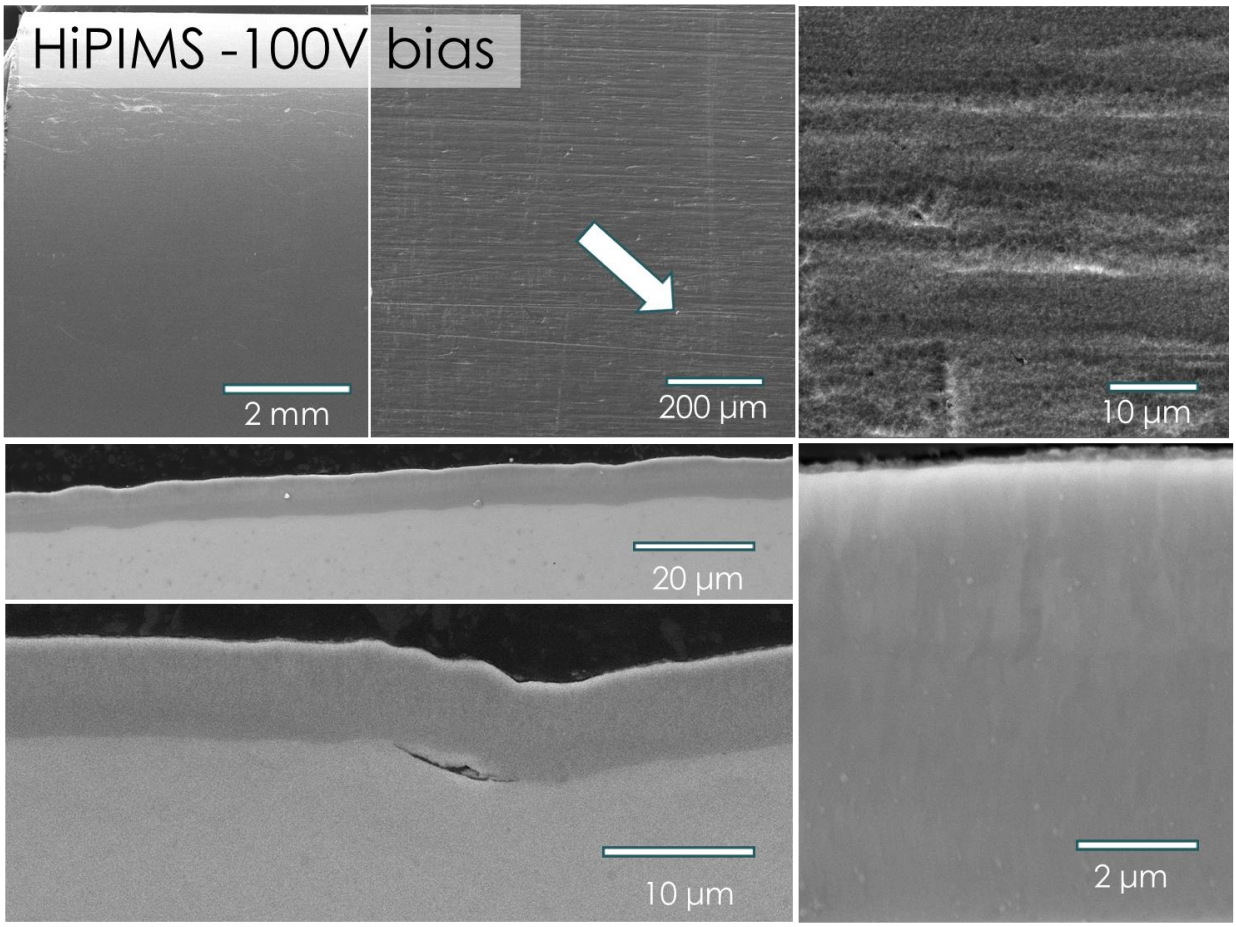

Figure 6 Top row: Radial view on the surface of the coating of sample -100 V bias on the substrate; Bottom row: Cross-section of the coating reveals a good adhesion and showing the largest defect in the cladding material is coated over.

Figure 6 shows the sample produced with a -100 V bias on the substrate. The surface of the sample shows a dense formed coating, while the macroscopic scratches from polishing the tubes are mirrored by the coating without cracking. That means that the coating grew less directional and that the Cr-ions had enough energy to fill the gaps between the directional growing grains of the coating. A white arrow is pointing at a position where abnormal Cr growth was found. This issue will be discussed in detail exemplarily on the -150 V sample, where those defects were found in higher numbers. The coating thickness is exhibited in the cross sections of the coating and was found to be 6.3 ±0.2 µm. The coating displays a good adhesion over the entire cross section. The only defect was found in the underlying cladding material, shown in the bottom left image in

Figure 6. This defect is either caused by the applied polishing process or is a remainder of the original surface. The elongated grain structure is faintly visible in the bottom right image of Figure 6, with smaller grains at the interface (bottom) and larger grain closer to the surface (top).

The investigation of the -150 V bias sample has revealed that this sample suffered from more abnormal Cr growth, highlighted by arrows in Figure 7. The largest identified abnormal growth was around 6.5 µm in diameter. The interface between the abnormal growth and the coating was investigated, tilting the sample to a 45° angle. The cladding material was not shown, which means that the coating may be not as thick at those interfaces, but no cladding is exposed in as-coated condition. During high temperature burst tests and further oxidation tests, the investigation of the abnormal growth and the behavior of the interface is crucial.

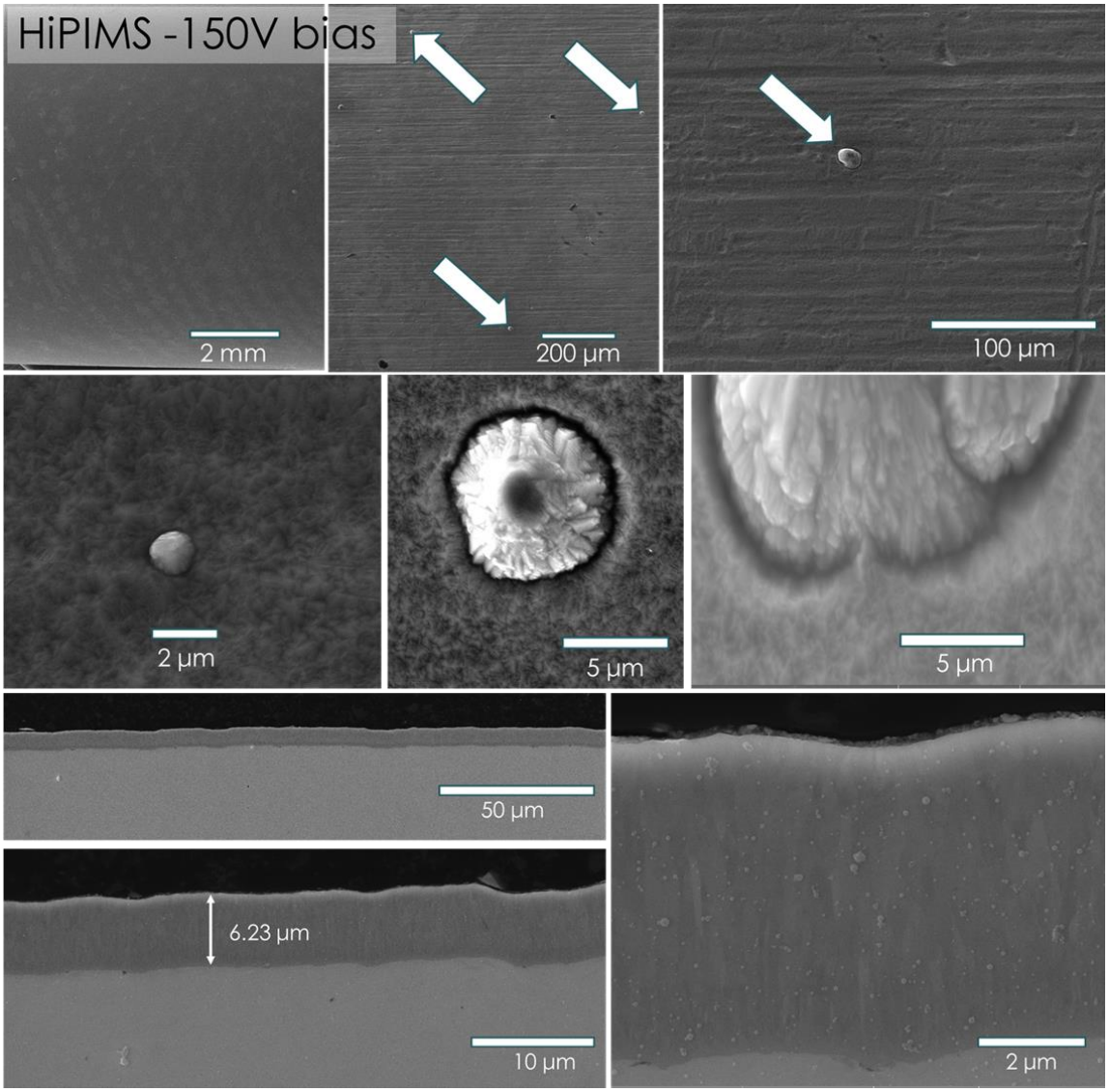

Figure 7 Top row: Radial view on the surface of the coating of -150 V bias sample showing abnormal Cr growth; Middle row: 2 examples of abnormal growth and a high magnification image of the interface between abnormal growth and the coating; Bottom row: Cross-section of the coating reveals a good adhesion and a coating thickness or around 6.23 ± 0.18 µm.

To determine if the abnormal growth of the coating is caused by the formation of a precipitate or a contamination, EDS SEM spot analysis and a map (not shown here) were recorded. The results of the spot analysis of the abnormal growth (Spot 1) and the adjacent normal coating (Spot 2) are shown in Figure 8. The only noticeable difference between the abnormal growth and the dense coating is the difference in the amount of oxygen, with the normal coating providing a higher oxygen peak. An EDS map did not show anything else other than Cr. Further investigation will determine if and how abnormal growth will impact the high temperate properties of the here shown Cr-coatings.

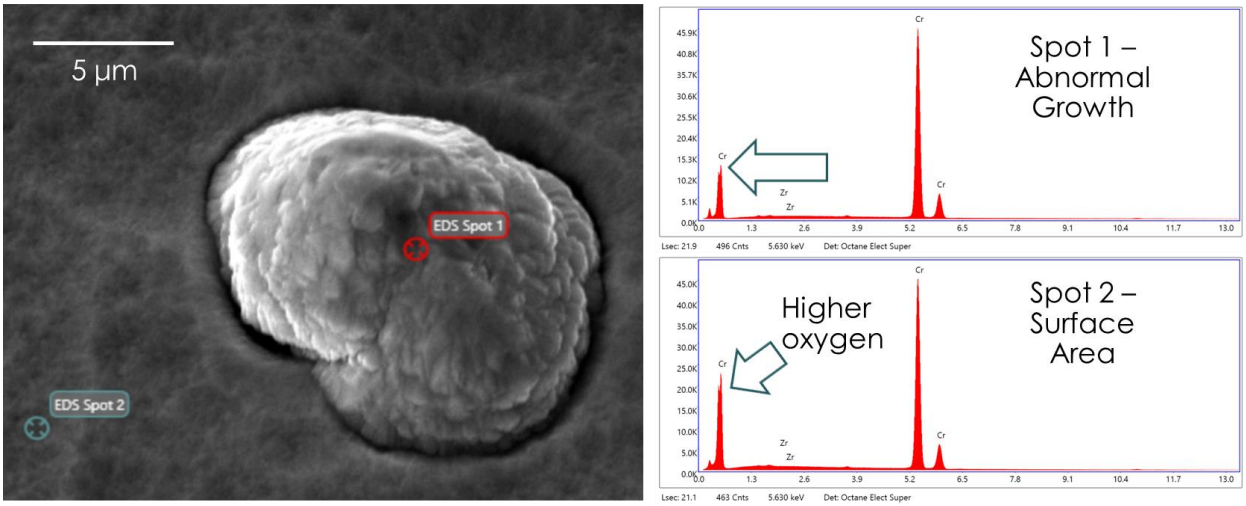

Figure 8 EDS SEM spot analysis of 2 locations to determine if the chemistry of the abnormal growth differs from the normal coating.

The results of the -200 V substrate bias coated tube are displayed in Figure 9. Interestingly, no clear trend was observed regarding the quantity of abnormally grown Cr in relationship to the chosen substrate bias. The lowest number was found at -100V, and the highest at -150 V, with -200 V in the middle. Island formation and abnormal growth is a phenomena which is caused by the substrate roughness, energy distribution of the ions, temperature, and bicollision events: the repulsion between the Cr-ions does not allow clustering, but some adatoms have higher energies than others and diffuse longer than others [11]. The bicollision event consists of local amorphization which fills the gaps between islands followed by crystallization due to secondary collisions and creates a smoother surface, which happens more often at higher energies. That means that island and abnormal growth can partly be controlled by an increased substrate bias and by a smoother original surface of the cladding [18]. Even though polishing of the cladding surface is possible, in large scale productions, the surface of the cladding will likely have some scratches or defects in local areas which could facilitate abnormal growth. The negative effect of an increased substrate bias is a considerable surface intermixing between coating and cladding, which favors the creation of a laves phase and higher compressive stresses in the cladding material. Recently it was demonstrated that the substrate bias has a direct impact on the residual stress in the film [11]. For that reason, the impact of those islands and the substrate bias on the overall properties need to be investigated. A recent report has highlighted those properties with the highest priorities [19]. A higher substrate bias leads to a dense coating, which potentially protects the cladding against oxidation and grid-to-rod-fretting [20,21]. Nanoindentation in combination with XRD to investigate the interface and residual stress will be performed in FY22.

A line scan across the interface of sample -150V bias was performed across 2.5 micron is shown in Figure 10. The elemental weight percentage of that scan is shown to the right side. At the interface an increase of Fe is visible which was found in the past to be an indicator of a formed laves phase [22][23]. Higher magnifications beyond the capabilities of an SEM are required to investigate the interface. TEM samples will be prepared of all samples and will be investigated in FY22.

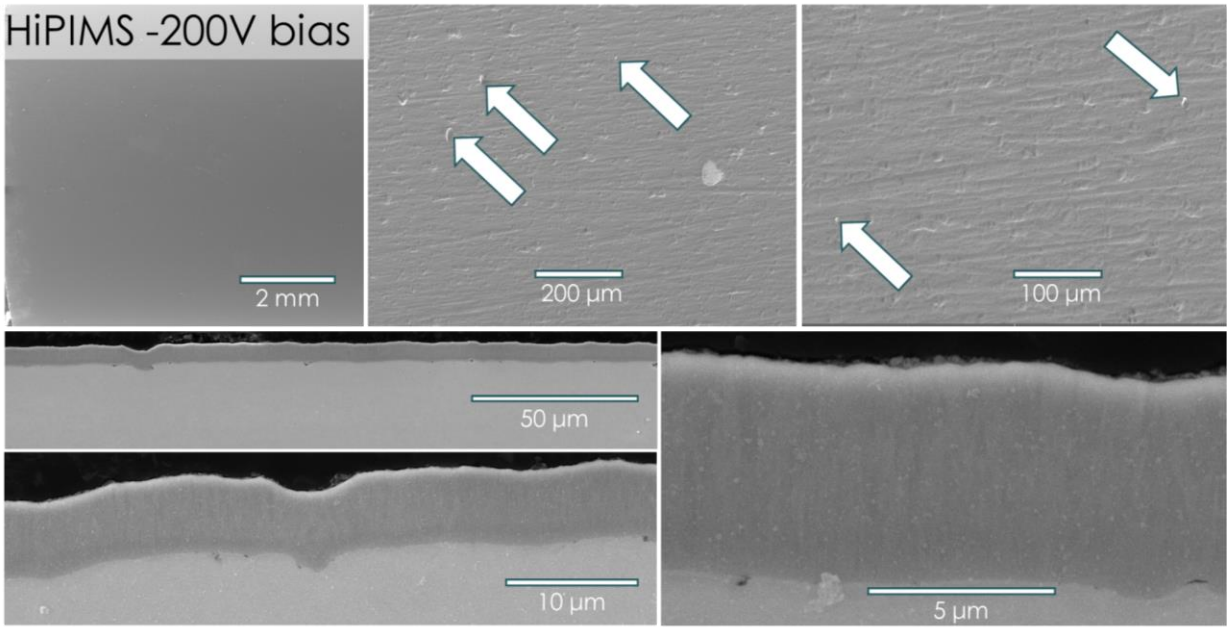

Figure 9 Top row: Radial view on the surface of the coating of sample -200 V bias on the substrate. Arrows point at some of the abnormally grown Cr clusters; Bottom row: Cross-section of the coating reveals a good adhesion.

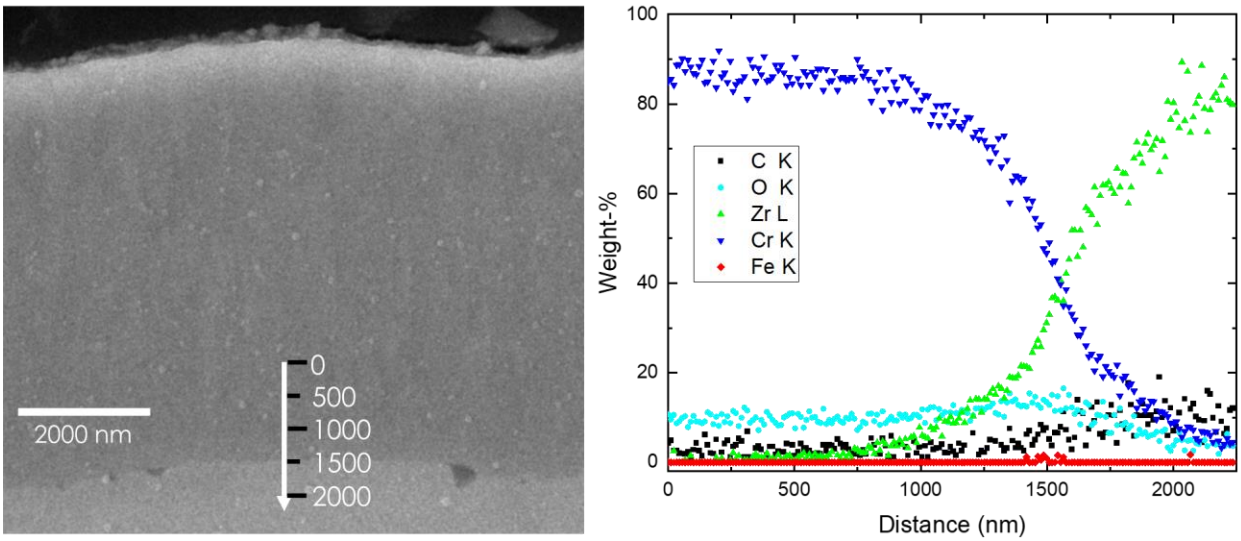

Figure 10 EDS line scan of the interface between Cr coating and Zry-4 cladding. A small increase of Fe at the interface is visible.

4. BURST TEST RESULTS

To evaluate the impact of Cr coatings on metrics representative of those needed to demonstrate accident tolerance, burst testing under simulated LOCA conditions was performed utilizing the severe accident test station (SATS) at ORNL. Detailed descriptions of the test procedure are given elsewhere [24,25].

In earlier studies comparing burst behavior of C26M FeCrAl to Zry-2 [25], burst temperatures and stresses were reported without denoted error, as C26M consistently burst at temperatures ~150°-200°C higher than Zry-2 at similar hoop stresses. However, any improvements to Zry-4 material strength imparted by a 5-10 μm Cr coating are assumed *a priori* to be small relative to that of the differences between C26M and Zry-2. Thus, a method of estimating burst temperature uncertainty is crucial for effecting useful comparisons of Cr coated Zry-4 and its bare counterpart. During LOCA testing, four thermocouples spanning the middle ~10 cm are used to monitor cladding temperature: (#1) one positioned azimuthally at 0° at approximately the middle axial length, (#2) one positioned azimuthally at 180°C, also at the middle axial length, (#3) one positioned azimuthally at 180°C but ~5 cm below #2 and (#4) one positioned azimuthally at 180° but ~5 cm above #2. The temperature profile is controlled through the temperature reading of #2, which is intentionally positioned in the IR furnaces hottest region. The location of burst typically occurs between #2 and #3, and #2 typically reads the highest temperature. However, the burst is sometimes located in the front of the cladding rather than the back, and at times #4 (the bottom TC) may read higher temperatures than #2 (the middle TC). To estimate burst temperature uncertainty, the absolute value of the difference between two thermocouples was recorded at burst for every presently discussed test, averaged, and divided by 2 (which assumes a linear gradient down the length of the cladding) and calculated to be 33°C. Thus, an error of ± 33°C is attached to all data points in the following discussion.

Previously, testing was conducted on 305 mm lengths of Zry-4 coated with a "poor" quality Cr coating that possessed interfacial and through-coating cracking resultant of a poor surface finish prior to deposition (Figure 3), along as 305 mm lengths of bare Zry-4 [15]. Although limited testing was performed, no improvement in burst strength, which manifests as higher burst temperatures at similar hoop stresses, was observed, Figure 11. Furthermore, both the poor quality Cr coated cladding (green triangles, red outline) and the bare Zr4 (green triangles) agree with Chapman's correlation (dotted grey line), which represents historical nuclear grade Zr alloy burst data [26,27].

The -100V bias HiPIMS Cr coated Zry-4 (Figure 6) was subjected to burst testing, and the relationship between burst temperature and hoop stress is also reported in Figure 11 (blue squares, red outline). Utilizing the aforementioned ± 33°C error, the 6-7 μm Cr coating (denoted as "good" quality coating) consistently burst at higher temperatures at similar stresses than the bare counterpart. However, due to a small supply of material, 153 mm lengths of coated cladding were tested as opposed to 305 mm lengths. The length dependance of burst is not yet a well understood relationship, so two 153 mm lengths of bare Zry-4 were tested (blue squares), yielding identical results to the bare 300 mm length Zry-4 (these two data points are overlapping in Figure 11)[28]. Additional 153 mm length bare Zry-4 testing will be performed, as well as replicate tests of the Cr coated claddings to statistically validate these positive preliminary findings.

Although exhibiting a relatively small but significant improvement in burst strength, cross sectional microscopy will still need to be performed to evaluate what impact the Cr coating had on reducing or entirely mitigating oxidation of the underlying Zry-4, as the formation of Cr_2O_3 in-lieu of ZrO_2 is viewed as the most critical factor when gauging improvements to accident tolerance imparted by Cr coatings. Presumably, the 'poor' coatings that have numerous flaws as visible in Figure 3 would allow for direct access of the oxidizing atmosphere to the Zry-4 substrate, resulting in performance that parallels that of the uncoated cladding. This will similarly require validation through microscopy.

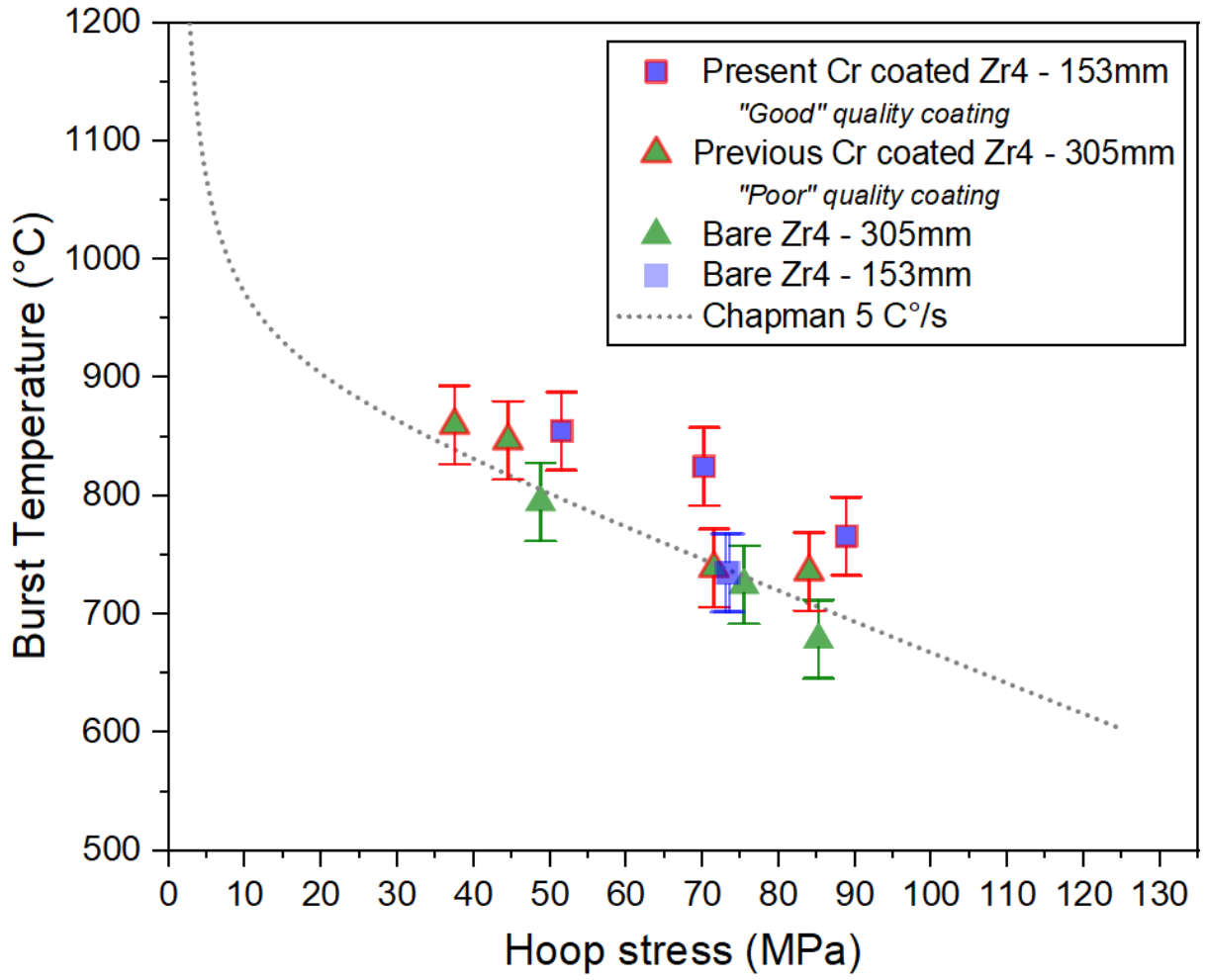

Figure 11 Relationship between burst temperature and hoop stress for several variations of bare and Cr coated Zry-4 cladding.

5. SUMMARY

Zry-4 tubes and have been coated with a 6 micrometer Cr coating using PVD HiPIMS methods. SEM investigations were performed on the surface and cross sections of the coated tubes to identify possible defects in respect to the three different substrate bias voltages used during the HiPIMS coating process. SEM images confirm that all three processing parameters were able to create a coherent and adhesive coating which mirrors the surface of the cladding material. No cracks were found in the coating; however, abnormal growth of Cr was found in some few locations. The quantity of the abnormal growth was highest on the -150V bias, second on the -200V bias, and lowest on the -100V bias coating. The -100V bias coated cladding was burst tested in comparison with the cracked coating and uncoated material.

Compared to bare Zry-4, the cracked coating imparted no benefit to burst strength, while the -100V bias coated cladding consistently burst at marginally higher, but significant, temperatures than bare Zry-4. Future FY22 work will be performed on HiPIMS coated Zry-4 tubes to investigate the impacts of the processing parameters on the residual stress, mechanical properties and the interface.

6. REFERENCES

[1] K.A. Terrani, Report on Design and Failure Limits of SiC/SiC and FeCrAl ATF Cladding Concepts under RIA Approved for public release, (2018).

[2] C. Tang, M. Stueber, H.J. Seifert, M. Steinbrueck, Protective coatings on zirconium-based alloys as accident-tolerant fuel (ATF) claddings, Corros. Rev. 35 (2017) 141–165. https://doi.org/10.1515/corrrev-2017-0010.

[3] M. Kurata, Research and Development Methodology for Practical Use of Accident Tolerant Fuel in Light Water Reactors, Nucl. Eng. Technol. 48 (2016) 26–32. https://doi.org/10.1016/j.net.2015.12.004.

[4] P. Hosemann, Small-scale mechanical testing on nuclear materials: bridging the experimental length-scale gap, Scr. Mater. 143 (2018) 161–168. https://doi.org/10.1016/j.scriptamat.2017.04.026.

[5] T. Shinozaki, Y. Udagawa, T. Mihara, T. Sugiyama, M. Amaya, Improved-EDC tests on the Zircaloy-4 cladding tube with an outer surface pre-crack, J. Nucl. Sci. Technol. 53 (2016) 1426–1434. https://doi.org/10.1080/00223131.2015.1123658.

[6] T. Jezequel, Q. Auzoux, D. Le Boulch, M. Bono, E. Andrieu, C. Blanc, V. Chabretou, N. Mozzani, M. Rautenberg, Stress corrosion crack initiation of Zircaloy-4 cladding tubes in an iodine vapor environment during creep, relaxation, and constant strain rate tests, J. Nucl. Mater. 499 (2018) 641–651. https://doi.org/10.1016/j.jnucmat.2017.07.014.

[7] H. Li, T. Koyanagi, X. Hu, Y. Katoh, Multiscale experimental characterization of coatings on ceramics: A case study of tungsten on SiC, Surf. Coatings Technol. 367 (2019) 1–10. https://doi.org/10.1016/j.surfcoat.2019.03.040.

[8] J. Chen, S.J. Bull, Approaches to investigate delamination and interfacial toughness in coated systems: An overview, J. Phys. D. Appl. Phys. 44 (2011). https://doi.org/10.1088/0022-3727/44/3/034001.

[9] H. Chen, X. Wang, R. Zhang, Application and development progress of Cr-based surface coating in nuclear fuel elements: II. Current status and shortcomings of performance studies, Coatings. 10 (2020). https://doi.org/10.3390/coatings10090835.

[10] A.-M. Velente-Feliciano, Hipims : A New Generation of Film Deposition Techniques for Srf Applications, Proc. SRF2013. (2013) 754–760.

[11] M. Kateb, J.T. Gudmundsson, S. Ingvarsson, Effect of substrate bias on microstructure of epitaxial film grown by HiPIMS: An atomistic simulation, J. Vac. Sci. Technol. A. 38 (2020) 043006. https://doi.org/10.1116/6.0000233.

[12] J.C. Brachet, I. Idarraga-Trujillo, M. Le Flem, M. Le Saux, V. Vandenberghe, S. Urvoy, E. Rouesne, T. Guilbert, C. Toffolon-Masclet, M. Tupin, C. Phalippou, F. Lomello, F. Schuster, A. Billard, G. Velisa, C. Ducros, F. Sanchette, Early studies on Cr-Coated Zircaloy-4 as enhanced accident tolerant nuclear fuel claddings for light water reactors, J. Nucl. Mater. 517 (2019) 268–285. https://doi.org/10.1016/j.jnucmat.2019.02.018.

[13] J. Ribis, A. Wu, J. Brachet, E. Clouet, B. Arnal, E. Rouesne, S. Urvoy, F. Barcelo, A. Gentils, C. Baumier, L. Rancoeur, Y. Robert, F. Leprêtre, J. Bischoff, E. Pouillier, Chromium hardening and Zr-Cr interface stability of irradiated chromium-coated

Zircaloy-4 alloy, (2018). https://hal-cea.archives-ouvertes.fr/cea-02400192 (accessed December 31, 2020).

[14] M. Wagih, B. Spencer, J. Hales, K. Shirvan, Fuel performance of chromium-coated zirconium alloy and silicon carbide accident tolerant fuel claddings, Ann. Nucl. Energy. 120 (2018) 304–318. https://doi.org/10.1016/j.anucene.2018.06.001.

[15] B. Garrison, K. Linton, K. Kane, S. Bell, T. Graening, C.S. Hawkins, B. Johnston, A.T. Nelson, AFC Burst Activities with Coated Zircaloy4 Under Accident Conditions, 2021.

[16] T. Graening, C.P. Massey, K. Linton, A. Nelson, Microstructure Investigation and Mechanical Properties of Coated Zircaloy Cladding, 2021.

[17] A.K. Evans, P.J. Kelly, D.T. Goddard, E.P. Vernon, Fabrication, characterisation and testing of cr coated zr alloy nuclear fuel rod cladding for enhanced accident tolerance, Light Water React. Fuel Perform. Conf. (TOP FUEL 2019). (2020) 864–872.

[18] M. Kateb, H. Hajihoseini, J.T. Gudmundsson, S. Ingvarsson, Role of ionization fraction on the surface roughness, density, and interface mixing of the films deposited by thermal evaporation, dc magnetron sputtering, and HiPIMS: An atomistic simulation, J. Vac. Sci. Technol. A. 37 (2019) 031306. https://doi.org/10.1116/1.5094429.

[19] T. Graening, P. Mouche, R. Sweet, P.L. Mulligan, K. Linton, A.T. Nelson, Development of Standardized Property Requirements , Measurement Methods , and Reporting Guidance for Coatings, 2021.

[20] C.C. Kuo, C.H. Lin, Y.T. Lin, J.T. Chang, Effects of cathode voltage pulse width in high power impulse magnetron sputtering on the deposited chromium thin films, Coatings. 10 (2020) 1–11. https://doi.org/10.3390/COATINGS10060542.

[21] C.C. Kuo, C.H. Lin, J.T. Chang, Y.T. Lin, Effect of voltage pulse width and synchronized substrate bias in high-power impulse magnetron sputtering of zirconium films, Coatings. 11 (2021) 1–13. https://doi.org/10.3390/coatings11010007.

[22] A. Wu, J. Ribis, J.C. Brachet, E. Clouet, F. Leprêtre, E. Bordas, B. Arnal, HRTEM and chemical study of an ion-irradiated chromium/zircaloy-4 interface, J. Nucl. Mater. 504 (2018) 289–299. https://doi.org/10.1016/j.jnucmat.2018.01.029.

[23] J. Ribis, A. Wu, J.C. Brachet, F. Barcelo, B. Arnal, Atomic-scale interface structure of a Cr-coated Zircaloy-4 material, J. Mater. Sci. 53 (2018) 9879–9895. https://doi.org/10.1007/s10853-018-2333-1.

[24] C.P. Massey, K.A. Terrani, S.N. Dryepondt, B.A. Pint, Cladding burst behavior of Fe-based alloys under LOCA, J. Nucl. Mater. 470 (2016) 128–138. https://doi.org/10.1016/j.jnucmat.2015.12.018.

[25] S.B. Bell, K.A. Kane, C.P. Massey, L.A. Baldesberger, D. Lutz, B.A. Pint, Strength and rupture geometry of un-irradiated C26M FeCrAl under LOCA burst testing conditions, J. Nucl. Mater. 557 (2021) 153242. https://doi.org/10.1016/j.jnucmat.2021.153242.

[26] R.H. Chapman, Multirod burst test program, Department of Energy,[Office of Energy Technology], Oak Ridge National …, 1978.

[27] D.A. Powers, R.O. Meyer, Cladding swelling and rupture models for LOCA analysis.

Technical report, Nuclear Regulatory Commission, 1980.

[28] B. Garrison, P. Champlin, M. Howell, M.N. Cinbiz, M.N. Gussev, C.M. Petrie, K. Linton, Progress Report on Length Dependence of Severe Accident Test Station Integral Testing, 2019.